Chromatographic separation of wood constituents

NIKLAS WESTERBERG

Chromatographic separation of wood constituents
NIKLAS WESTERBERG

Department of Chemical and Biological Engineering
Chalmers University of Technology
SE-412 96 Göteborg, Sweden

Chromatographic separation of wood constituents

Niklas Westerberg
Chemical Engineering
Department of Chemical and Biological Engineering
Chalmers University of Technology
SE-412 96 Göteborg, Sweden

Abstract

This thesis investigates the potential and limitations of using chromatographic separation to purify fractions of biopolymers extracted from wood.

Hot-water-extracted Norway spruce was fractionated by cross-flow filtration followed by two stages of hydrophobic adsorption with increasing hydrophobic selectivity. Three fractions were recovered and characterized according to Klason and sugar content, and by size exclusion measurements of enzymatically hydrolyzed samples, revealing species covalently bound to carbohydrates. The fractions were mainly characterized by the amounts of aromatic species, where the first fraction contained about 56 % lignin, the second contained about 10 % lignin and the third about 1.5 % lignin. The non-lignin part of the fractions consisted of hemicelluloses, mainly galactoglucomannan. The method investigated proved successful in separating lignin, LCCs and carbohydrates with mild processing that did not affect the molecular structure of the species.

A mathematical model describing the migration of wood model constituents in a chromatographic column has been developed. A combination of the frontal analysis (FA) method and pulse injection breakthrough measurements were used to estimate the parameters that describe solute migration for a simplified model system. The parameters estimated pertained to the mass transport phenomena of axial dispersion, film mass transfer and particle diffusion. The hydrophobic affinity parameters were also determined in the forms of isotherms and the effect of an organic mobile phase modifier. In addition, the packed-bed parameters of bed porosity and particle porosity were determined. The model accuracy was verified to be within 95 %. The particle pore size is suspected of limiting the capacity of the sorbent. Moreover, the relatively small particle sizes used (68 μm) induce quite a high pressure drop over the column which must be optimized in a large-scale process.

Acknowledgments

I would like to take this opportunity to express my gratitude to all of those who helped me finish writing this thesis.

First I want to thank Professor Anders Rasmuson for giving me the opportunity to do my PhD at Chalmers, and for the time he has spent encouraging me and for the technical issues he has helped me solve.

To my roommate Björn, for all the tips and tricks you have taught me in MatLab, and for introducing me to Me-Me:s.

All the staff at KAT/KRT and SIKT for technical assistance at the many laboratories I have used.

A special thanks to all my fellow PhD students at Chalmers and within the Wallenberg Wood Science Centre, with whom I have shared the trials and tribulations of our work, and to the staff that have encouraged us in times of darkness.

Lastly, I want to thank my girlfriend for moral support, for doing the weekend dishes while I was stuck at work, and for delicious chocolate pastries.

List of Publications

The work of this thesis is based on the following pubilcations:

- **Separation of galactoglucomannans, lignin, and lignin-carbohydrate complexes from hot-water-extracted norway spruce by cross-flow filtration and adsorption chromatography**
  Niklas Westerberg, Hampus Sunner, Mikaela Helander, Gunnar Henriksson, Martin Lawoko, and Anders Rasmuson
  Published in *Bioresources* 7(4), 4501-4516, 2012

- **Chromatographic separation of wood model constituents - Mathematical modeling and parameter estimation**
  Niklas Westerberg and Anders Rasmuson
  In manuscript

Contents

1

Introduction

1.1 General problem area

Concerns have been raised that the rate at which oil can be extracted from the ground has already peaked, or is likely to do so early in the 21st century (ASPO [1]). To meet the shortage of resources that will follow this event, there is a general research interest to find ways to replace the petrochemical feedstock with renewable resources. Wood is a renewable resource available in vast quantities, and initiatives are underway to develop new, advanced products and materials from wood. The Wallenberg Wood Science Centre (WWSC) is a joint research centre between the Royal Institute of Technology (KTH) in Stockholm and Chalmers University of Technology in Gothenburg. In 2009, the WWSC launched a material research programme aimed at developing new materials from industrially viable wood species found in Scandinavia. The WWSC was formed by a donation made by the Knut and Alice Wallenberg Foundation (WWSC [2]).

A number of new material applications of wood polymers have been described and are under development. Examples of uses are hydrogels (Lindblad et al. [3]) and gas barrier films for food packaging, produced both with the hardwood-abundant xylan (Grondahl et al. [4]) and softwood-abundant galactoglucomannans (GGM) (Hartman et al. [5]). Besides the three common components of wood (cellulose, hemicellulose and lignin), studies of the composition of dissolved wood have also found lignin covalently bound to sugars

(Bjorkman [6], Koshijima and Watanabe [7], Azuma et al. [8], Lawoko et al. [9]). Whether these structures exist in native wood, or if this is an artifact of processing is still being debated. The term lignin-carbohydrate complex (LCC) was introduced by Bjorkman [6]. These structures have also presented potential technical applications. Uraki et al. [10] investigated the amphiphilic properties of LCCs and suggested the potential use of LCCs as a polymeric surfactant or as a substance carrier in pharmaceuticals. In addition, Oinonen [11] reports on a method for synthesizing LCC structures and has measured the oxygen barrier properties of polymerized LCC and found them to be similar to the properties of synthesized hemicellulose. LCC is thought to be very diverse in molecular weight and to have aromatic branching on a polysaccharide backbone. If these structures could be separated into pure fractions not only by molecular size, but also by the ratio of aromatic to carbohydrate constituents, more specific material characteristics could be developed. One prerequisite of material production from wood polymers is the development of methods to separate wood constituents.

Commonly employed techniques to achieve such separation are filtration (Persson et al. [12], Andersson et al. [13]) and precipitation (Lawoko et al. [9]). The use of filtration is restricted by being chemically nonspecific. Biopolymers from wood can thus only be separated by filtration into fractions of molecules of equal size. Since hemicelluloses and fragments of lignin are often found in the same region of molecular weight, filtration is of very limited use when pure fractions of biopolymers are desired. Precipitative separation is based on the solubility of molecules in various solvents. The solubility of a polymer is mainly attributed to its chemical structure, making precipitation a chemically specific method of separation. However; small polymers are less prone to precipitate, and polymers that have a combination of chemical structures have a solubility that differs from pure species. Moreover, precipitation can be irreversible, rendering the precipitated species useless. A third method of separation is sorption. Sorption utilizes the interaction forces between solute species and a solid material that make the species interact (*sorb*) with the surface of the solid phase. Sorption has a much higher chemical specificity than precipitation, but is far more costly. The use of sorptive separation to remove aromatic substituents from industry waste waters has been summarized in Lin and Juang

[14].

It can be concluded that there is a need to develop non-destructive, selective methods to achieve separation of wood constituents. With regard to the purity of the purified fractions; chromatography is probably the method with the greatest potential. The very high specificity of chromatography makes the process suitable for analytical purposes, but it is not extensively employed in biorefinery for production purposes due to the high costs associated with the separation process. Therefore need for further knowledge is needed about the possibilities and limitations of the chromatographic separation of wood constituents, and the development of models to be able to analyze the tradeoff between productivity and fraction purity, and to scale up the process.

1.2 Objectives

The objective of this thesis is to investigate the potential and the limitations of using chromatographic separation to purify fractions of wood constituents.

The performance of separating hot-water-extracted wood constituents with a simple experimental setup, consisting of cross-flow filtration followed by two sequential stages of hydrophobic adsorption, was evaluated by analysing the chemical structure of the components captured between each stage. Focus was on distinguishing molecules classified as either lignin, carbohydrate or as a lignin-carbohydrate-complex.

Wood model constituents were used to estimate the effect of axial dispersion, film mass transfer, diffusivity and adsorption equilibria in reversed phase chromatography. Experiments combined with parameter fitting resulted in a mathematical model of the system. The model can be used to evaluate the restricting parameters of the separation procedure and to find optimal operating conditions.

1.3   Outline of the thesis

Chapter 2 gives an overview of the theoretical background of the thesis. The basics of wood constituents, and the concepts of chromatography and adsorption are explained, followed by a presentation of relevant transport mechanisms. The mathematical model used in the work is thoroughly explained in Chapter 3. Chapter 4 explains the experimental setup used for this thesis and the parameter estimation. Some example results of the studies are shown in Chapter 5 and the conclusions from the investigations are summarized in Chapter 6. The two papers this thesis is based on include more detailed information and are attached last.

2

Background

2.1 Wood and wood constituents

The focus of this study is on biorefining constituents from wood. Trees are usually categorised into two kinds: softwood (conifers), and hardwood (deciduous or broad-leaf). In Scandinavia, the trees of the most industrial significance are the conifers; Scots pine (Pinus sylvestris) and Norway spruce (Picea abies). This study is focused on the latter; Norway spruce.

Wood consists of cellulose, hemicelluloses, lignin, wood extractives and some inorganic material. The general composition of these constituents in softwood is 40-46 % cellulose, 23-30 % lignin and 19-26 % hemicelluloses with the remaining few percentages made up of extractives and inorganics (Ek [15]). Investigations into the composition of dissolved wood have also found lignin covalently bound to sugars (Bjorkman [6], Koshijima and Watanabe [7]; Azuma et al. [8]; Lawoko et al. [9]). Whether these structures exist in native wood or if this is an artifact of processing is still being debated. The term lignin-carbohydrate complex (LCC) was introduced by Bjorkman [6]. The findings of Lawoko et al. [9] have even suggested that all hemicelluloses in wood are covalently bound to lignin.

Cellulose, which is the most common compound found in wood, provides structural support in trees. The molecule is a polymer, consisting of 800-10000

repeating units of $\beta - D - glucose$. The number of repeating units is commonly referred to as the *degree of polymerisation* (DP), and this degree decreases during pulping to 300-1700 (Ek [15]). The repeating unit and the low amount of side groups makes the cellulose polymer orient in a crystalline manner, which provides the basis of the strength and support in wood.

Hemicelluloses are also polymers that consist of sugar monomers. The DP of hemicelluloses is much lower than that of cellulose, typically around 100-200. The low DP and the high degree of branching of the polymers makes the hemicellulose network structure rather amorphous. The dominant hemicellulose found in Norway spruce is *galactoglucomannan*, a polymer that consists of monomers of mannose, glucose and galactose, listed here in order of decreasing frequency.

Lignin is a complex polymer oriented in a, seemingly, random network of phenyl propane units. Lignin functions as an adhesive that glues components together into a substance that we call wood.

Lignin-carbohydrate complexes (LCCs) are hemicelluloses that have covalently bonded to lignin sidegroups. The structure, or even existence, of native LCCs is unknown. However, LCCs are usually found in pulping extracts and Lawoko et al. [9] has characterized LCCs as present in the residue of mildly ball-milled wood. LCCs are thought to be widely dispersed in DP as well as in the amount of lignin constituents attached to the hemicellulose backbone.

2.2   Chromatography

Chromatographic separation setups always consist of a mobile phase, a fluid, in which the molecules, *solutes*, are transported, and a stationary phase, which the molecules interact with. In liquid chromatography (LC) the stationary phase is usually particulate and contained in a stainless steel column. Figure 2.1 depicts the mobile-phase flow entering the column and flowing in different pathways between the particles. The particle surface is usually treated to contain molecular groups, *ligands*, of specific characteristics to have strong interactions with the molecules that are to be separated. The interaction only occurs when the solutes in the mobile phase come in close contact with the ligands of the stationary phase. Then a weak momentary bonding occurs be-
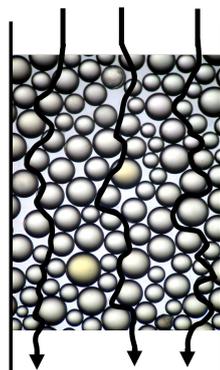
Figure 2.1: Flow through a packed bed

tween solute and ligand (adsorption), before the solute is rereleased into the mobile phase (desorption). The strength of the interaction between solute and ligand varies with the chemistry of the solute and the ligand, and also with the chemistry of the mobile phase. Figure 2.2 depicts the migration of two solutes through a chromatographic column.

In this example, the solute indicated by light gray has weak interaction with the ligands and is therefore, by preference, located in the mobile phase. The solute indicated by dark gray, however, has strong interactions with the ligands and is therefore retained in the column.

This example is a simplified explanation of chromatography. More detailed descriptions of the transport processes that occur in the column and adsorption kinetics are found below.

2.2.1   Reversed phase chromatography

The separation mechanism in reversed-phase chromatography (RPC) is based on hydrophobic interaction between the hydrophobic solutes in the liquid phase and the immobilized hydrophobic ligands in the stationary phase. The hydrophobic interaction is greater if both the ligands and the solutes are of a phenylic character, due to interaction between π electrons.
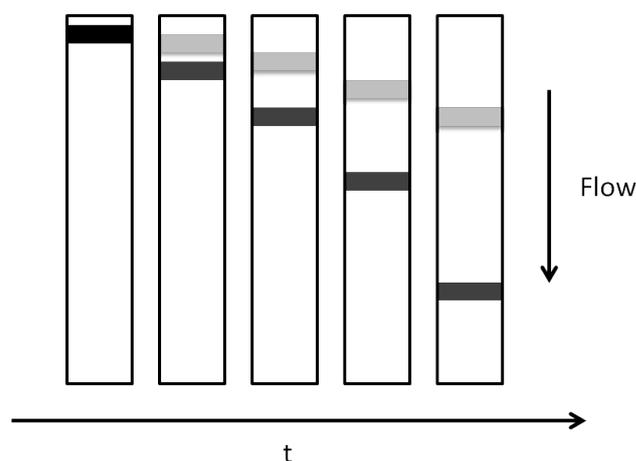
Figure 2.2: Components migrate through the packed bed with different speed, due to interaction with the stationary phase

2.3   Adsorption

When discussing the fundamentals of adsorption, it is necessary to distinguish between *physical* adsorption and *chemical* adsorption. *Chemisorption* essentially involves the formation of chemical bonds between the sorbate molecule and the surface of the adsorbent. *Physisorption* involves only relatively weak intermolecular forces, making physical adsorption reversible while chemisorption is often an irreversible reaction.

The distinction between physical and chemical adsorption is conceptually useful, but there are many intermediate cases that might be impossible to categorize exclusively in either of the two cases. Almost all adsorptive separation processes depend on physical adsorption, rather than chemical sorption. This thesis focuses on physical adsorption.

The forces involved in physical adsorption include both Van der Waal, dispersion/repulsion forces, and electrostatic interactions comprising polarization, dipole, and quadropole interactions. Ruthven [16] lists the equations describing these interactions along with a thorough explanation of the process

2.3.1   Adsorption equilibrium

Adsorption is a dynamic process where molecules in solute state continuously transfer to the adsorbed state, and vice versa. In the simplest model of ad-

sorption, where the surface is energetically uniform and there is no interaction between the adsorbed molecules, the rate of adsorption, with first-order kinetics, can be expressed as:

$$k_{ads}C(1 - \Theta) \tag{2.1}$$

$$\Theta = q/q_0 \tag{2.2}$$

where C is the solute concentration in the liquid state, q is the concentration in the adsorbed state and k_{ads} is a constant. q_0 is the adsorption capacity of the sorbent. Correspondingly, the rate of desorption can be expressed:

$$k_{des}\Theta \tag{2.3}$$

With time, the concentration in the two phases will reach equilibrium, when the rate of adsorption equals that of desorption.

$$k_{ads}C(1 - \Theta) = k_{des}\Theta \tag{2.4}$$

Expressing the rate constants relation as

$$K = \frac{k_{ads}}{k_{des}} \tag{2.5}$$

gives Equation 2.6 that relates the concentration in the solute state to the concentration in the adsorbed state at equilibrium.

$$\theta = \frac{K \cdot C}{1 + K \cdot C} \tag{2.6}$$

Equation 2.6 is called the Langmuir isotherm. For very low values of q, Equation 2.6 is reduced to the Henry-type, linear, equation

$$\theta = K \cdot C \tag{2.7}$$

Furthermore, the sorbent becomes saturated at high concentrations ($\theta = 1$).

A number of modifications of the Langmuir isotherm have been proposed to better fit experimental data. The modifications concern additional interaction energies or the surface structure of the sorbent. The experimental data of

this thesis was fitted to a number of isotherms, with the best fit to the Tóth
isotherm, Equation 2.8.

$$q_i = k_2 \left(\frac{1}{(KC_i)^{k_3}} + 1 \right)^{-\frac{1}{k_3}} \tag{2.8}$$

The Tóth isotherm accounts for adsorption on a heterogeneous surface, with no
adsorbate-adsorbate interaction. The heterogeneous surface is assumed to have
a unimodal adsorption energy distribution in an interval related to the value
of parameter k_3. The Tóth isotherm was first derived for gas-solid equilibria,
but like the Langmuir isotherm, it can be extended to liquid-solid equilibrium,
Guiochon et al. [17].

2.4   Transport mechanisms

There are a number of transport mechanisms relevant for chromatographic op-
eration. They include: flow, axial dispersion and external/internal mass trans-
fer. Axial dispersion and mass transfer kinetics in general cause a broadening
of the concentration pulse.

2.4.1   Axial dispersion

There are two main mechanisms that contribute to axial dispersion: molecular
diffusion and the flow velocity distribution in the porous bed. In a first ap-
proximation these effects are additive so that the dispersion coefficient may be
represented by Equation 2.9.

$$D_{A,x} = D_M + D_H \tag{2.9}$$

where $D_{A,x}$ is the total dispersion, D_M is diffusivity and D_H is the hydrody-
namic contribution. In liquid systems, the molecular diffusivities are too small
to make any significant contribution to axial dispersion, even at low Reynolds
numbers (Ruthven [16]).

$$D_{A,x} \approx D_H \qquad \text{(liquid systems)} \tag{2.10}$$

If the ratio of bed-to-particle diameter is not sufficiently large the dispersion might increase significantly from wall effects and from non-uniform packing Guiochon et al. [17].

Chung and Wen [18] has reviewed a great amount of published data concerning dispersion in fixed beds and has found an expression to estimate the Peclet number as a function of the Reynolds number.

$$(Pe\varepsilon_c)/X = 0.2 + 0.011Re^{0.48} \tag{2.11}$$

$$Re = \frac{u_0 d_p}{\nu} \tag{2.12}$$

$$Pe = \frac{u_0 d_p}{D_{A,x}} \tag{2.13}$$

where u_0 is the interstitial velocity through the column and X is equal to unity for fixed beds. The correlation by Chung and Wen [18] is applicable over a porosity range of 0.4 to 0.8 with particle density up to 7700 kg/m^3 and Reynolds number ranging from 10^{-3} to 10^3. This is the most widely used correlation for estimating dispersion in a chromatographic column when no experimental procedure is available.

2.4.2 Relative importance of internal and external resistances

Large-scale adsorption processes have the practical implication of maintaining a reasonable pressure drop at the relatively high flow rates required. From a process design perspective this is achieved by using particles with a relatively large diameter in the fixed bed setup. If the interior of the particles has a hierarchical structure, then several diffusive resistances can be distinguished, in addition to external film resistance. Any single resistance, or more likely; any combination of these different resistances may control the rate of mass transfer, or at least may have a significant effect on it.

The dimensionless Biot number measures the ratio of internal to external mass transfer resistance, and is defined (for spheres) in Equation 2.14

$$Bi = \frac{k_c d_p}{6\varepsilon_p D_p} \tag{2.14}$$

or in terms of the Sherwood number

$$Bi = \frac{ShDe}{6\varepsilon_p D_p} \tag{2.15}$$

Ruthven [16] argues that since $Sh \geq 2$ and $Dp \leq Dm/\tau$ (where τ is the tortuosity factor, ≥ 1) the minimum value of Bi is $\tau/3\varepsilon_p$ (≈ 3.0). Thus, even at these rather extreme conditions, the internal gradient is clearly larger than the external. Any additional effects such as Knudsen diffusion or intra-crystalline diffusion would add to the internal mass transfer resistance. Based on these arguments it may be concluded that intra-particle resistance is likely to provide the dominant resistance that restricts the rate of mass transfer.

2.4.3   Film mass transfer

The external fluid film resistance around the particles is determined by the hydrodynamic conditions. The condition of no slip at the solid boundary means that each particle is surrounded by a laminar sub layer. Mass transfer between the bulk fluid and the solid particle is by molecular diffusion through this sub layer. The rate of mass transfer is thus determined by the thickness of the sub layer and is more conveniently expressed by an effective mass transfer coefficient, kf, which is determined by the hydrodynamic conditions. According to a linear driving force equation the coefficient is expressed as

$$V\frac{\partial q}{\partial t} = k_c a_s (C - C^*) \tag{2.16}$$

where a_s is the external surface area, V is the control volume, q is the adsorbed phase concentration averaged over the control volume. The Sherwood number is a dimensionless group characterizing film mass transfer

$$Sh = \frac{d_p k_c}{D_e} \tag{2.17}$$

where R_p is the particle radius and D_e is the molecular diffusivity coefficient of the molecule in question in the liquid. As Sh is analogue to the Nusselt

number for heat transfer a lower limiting value of $Sh = 2$ can be found when the particle is surrounded by a stagnant fluid. In a fluid flow the Sherwood number is expressed as a function of the Reynolds number and the Schmidt number. For the low values of the Reynolds number in chromatography the empirical correlation of Wilson and Geankoplis [19] is useful:

$$Sh = \frac{1.09}{\varepsilon_c}(Re \cdot Sc)^{0.33} \quad 0.0015 < Re < 55 \tag{2.18}$$

2.4.4 Diffusion

The process in which a concentration gradient is eliminated by random molecular movement, self-propelled by thermal energy, is called *diffusion*. According to Fick's law (Fick [20]), the diffusion flux is proportional to the negative gradient of concentration. Molecules move from regions of higher concentration to regions of lower concentration. A distinguishing feature of diffusion is that it results in mixing or mass transport without requiring any bulk motion.

There are two commonly encountered correlations for estimating the diffusivity of a dilute specie in a liquid. Most common is the Stokes-Eintein equation, especially for large molecules such as proteins or polymers.

$$D = \frac{k_B T}{6\pi\mu R_s} \tag{2.19}$$

k_B is the Boltzmann constant, T is the temperature and R_s is the Stokes radius (hydrodynamic radius) of the diffusing molecule.

$$R_s = \left(\frac{3M_W}{4\pi\rho N_A}\right)^{1/3} \tag{2.20}$$

Wilke and Chang [21] derived a useful, semi-empirical, expression from large amounts of experimental data, and is often found in contexts of chromatography, Equation 2.21.

$$D_{AB} = 7.4 \times 10^{-8}\frac{(\phi_B M_B)^{1/2}T}{\eta_B V_A^{0.6}} \tag{2.21}$$

where ϕ_B is the association number of the solvent, $M_{W,B}$ is the molecular weight of the solvent, T is the temperature in $^\circ K$, η_B is the solvent viscosity in cP and V_A is the molal volume of the diffusing specie, in cm^3/mol.

Diffusion in porous media

The deviation from simple equilibrium between the mobile and the stationary phase is usually not a result of the kinetics of adsorption and desorption, but rather a result of the transport of solutes between bulk liquid and a vacant site for adsorption. Following the argument of the limiting case of the Biot number above combined with the longer diffusion distances resulting from reducing pressure drop over a fixed bed by increasing the diameter of the particles, - diffusion in porous media might be the most important parameter to control.

In contexts of diffusion inside porous structures, a distinction is often made between two separate diffusion phenomena: *macropore* diffusion and *micropore* diffusion (Ruthven [16], Suzuki [22], Guiochon et al. [17]). Micropore or intracrystalline diffusion occurs in the volume of the solid, where the diffusing molecule never escapes the force-field of the adsorbent surface. Macropore diffusion takes place in the fluid that fills the pores of the particles. Guiochon et al. [17] complicates the definition even further by stating the micropores have diameters smaller than 2 nm, macropores have diameters larger than 50 nm, and classifying everything in between as *mesopores*. It might be easier to grasp the difference between macro- and micropores from the hierarchical structure of the adsorbents; most commercial adsorbents consist of small microporous crystals that are formed into macroporous pellets or particles.

For macropore diffusion Ruthven [16] distinguishes four separate mechanisms of transport:

1. Molecular diffusion; diffusion in liquid filled pores, where the liquid diffusion coefficient must be corrected with a tortuosity factor to account for three effects that restrict the diffusional flux: i) the random orientation of the pores, which leads to a longer diffusion path than a straight pore would, ii) a reduced concentration gradient in the direction of flow, iii) the variation in pore diameter that, locally, accelerates the flow.

$$D_p = D_e/\tau \qquad\qquad (2.22)$$

2. Knudsen diffusion; when the pore of diffusion is so narrow that the molecule frequently collides with the wall, thereby reducing velocity.

3. Poiseuille flow; when there is a pressure gradient over the particle inducing an additional acceleration that adds to the diffusional flux. This effect is generally insignificant since the flow resistance in the particles is very large in chromatography.

4. Surface diffusion; refers to when a molecule never leaves the force field of the sorbent surface, but instead jumps between sites available for adsorption. This constricted means of diffusion might make a significant contribution to the flux if the concentration on the surface is very high. The effect is more pronounced if the other acting diffusion is dominated by Knudsen diffusion.

Micropore diffusion occurs by means of the same mechanism as surface diffusion, except in a three-dimensional network in the small micropores, rather than in the larger macropores where this transport takes place on the surface of the pores.

2.4.5 Flow and pressure drop

Pressure drop in flow through fixed beds has been investigated by a number of authors. Some have made a significant contribution to the application at hand and deserve to be mentioned. Darcy (Darcy [23]) related the pressure drop to the liquid flow through an incompressible bed, Equation 2.23.

$$u = \frac{K}{\mu} \frac{\Delta P}{\Delta z} \tag{2.23}$$

where u is the superficial flow velocity through the bed, μ is the dynamic viscosity of the fluid, ΔP is the pressure drop over the bed when Δz is the length of the bed. K is the permeability of the bed.

In chromatographic contexts, two other frequently referred to investigations related to pressure drop in fixed beds are Chilton and Colburn [24] and Ergun [25]. The data from these and other authors show considerable scatter, although with a common general trend. The scatter is most likely due to wall effects or differences in bed voidage in the different investigations. The data may be conveniently correlated in terms of a dimensionless friction factor, f, defined by Equation 2.24.

$$f = \left(\frac{d_p}{L}\right)\frac{\Delta P}{\rho_f(\varepsilon_c u_z)^2} \tag{2.24}$$

where Δp is the pressure drop (Pa), L is the length of the packed bed, d_p is the diameter of the particulate packing material, ρ_f is the density of the fluid and εu_Z is the superficial fluid velocity.

Chilton-Colburn:

$$f = \begin{cases} 805/Re & \text{Re} < 40 \\ 38/Re^{0.15} & \text{Re} > 40 \end{cases} \tag{2.25}$$

Ergun:

$$f = \left(\frac{1-\varepsilon_c}{\varepsilon_c^3}\right)\left[\frac{150 \cdot (1-\varepsilon_c)}{Re} + 1.75\right] \tag{2.26}$$

Both correlations use the Reynolds number based on particle diameter and superficial fluid velocity. Although the expressions are quite different, they show close numerical agreement for a bed voidage of about 0.35. The pressure drop can be significantly reduced due to wall effects; unless the bed diameter is large relative to the particle diameter.

3

Mathematical model

3.1 The column

The column is modeled as a cylinder filled with particles of equal size. The fluid that flows through the column by means of convection is subjected to small-scale mixing, termed axial dispersion, and is physically depicted using the parameter $D_{A,x}$ (m^2/s).

A shell balance over a thin slice of the column with a constant cross sectional area A (m^2) and a thickness Δ x (m) is used to solve the mass balance for a component in the mobile phase (see fig. 3.1). It is assumed that the packing of the particles is uniform and that the void fraction is independent of the position in the column. Furthermore, adsorption is assumed to occur only inside the particles and is thus solved using a shell balance over the particles (see next subsection). The mass balance for the thin slice is as follows:

$$IN + PRODUCTION = OUT + ACCUMULATION \qquad (3.1)$$

Since no reaction occurs in the mobile phase the term PRODUCTION is set to zero. The component is transported in and out of the control volume by means of convection and axial dispersion. Within the control volume, the component is also transported between the mobile phase and the particles of the sorbent. The accumulation term, ACC, is thus a result of the net transport of the component in the control volume.

17

$$ACC = (IN - OUT)_{Conv} + (IN - OUT)_{Disp} + (IN - OUT)_{Particle} \quad (3.2)$$

The various terms are defined as:

$$ACC = \varepsilon_c \cdot A \cdot \Delta x \cdot \frac{\partial C}{\partial t} \quad (3.3)$$

$$(IN - OUT)_{Conv} = (u_0 \cdot \varepsilon_c \cdot A \cdot C)_x - (u_0 \cdot \varepsilon_c \cdot A \cdot C)_{x+\Delta x} \quad (3.4)$$

$$(IN - OUT)_{Disp} = \left(-D_{A,x}\varepsilon_C A\frac{\partial C}{\partial x}\right)_x - \left(-D_{A,x}\varepsilon_C A\frac{\partial C}{\partial x}\right)_{x+\Delta x} \quad (3.5)$$

$$(IN - OUT)_{Particle} = -(1 - \varepsilon_c)A\Delta x\frac{6}{d_p}k_c(C - C_{p,R}) \quad (3.6)$$

where x is the axial coordinate of the column (m), C is the concentration of the solute in the mobile phase (mol/m^3), $6/d_p$ is the specific area of the particles in relation to their volume (m^2/m^3), $C_{p,R}$ is the concentration of the solute at the particle surface (mol/m^3), A is the cross sectional area of the column (m^2), ε_c is the interstitial porosity of the column (m^3/m^3), k_c is the film mass transfer parameter (m/s), Δx is the length of the thin slize (m) and t is the time (s).

Inserting Equations 3.3 - 3.6 in 3.2 gives the following mass balance:

$$\varepsilon_c \cdot A \cdot \Delta x \cdot \frac{\partial C}{\partial t} = \left(-D_{A,x}\varepsilon_C A\frac{\partial C}{\partial x}\right)_x - \left(-D_{A,x}\varepsilon_C A\frac{\partial C}{\partial x}\right)_{x+\Delta x}$$

$$-(u_0 \cdot \varepsilon_c \cdot A \cdot C)_x - (u_0 \cdot \varepsilon_c \cdot A \cdot C)_{x+\Delta x} - (1 - \varepsilon_c)A\Delta x\frac{6}{d_p}k_c(C - C_{p,R})$$

Division by $\Delta x\varepsilon_c A$ and letting $\Delta x \to 0$ results in Equation 3.7, commonly referred to as the General Rate Model (GRM) (Guiochon et al. [17]).

$$\frac{\partial C}{\partial t} = -u_0\frac{\partial C}{\partial x} + D_{A,x}\frac{\partial^2 C}{\partial x} - \frac{1 - \varepsilon_c}{\varepsilon_c}\frac{6}{d_p}k_c\left(C - C_s\right) \quad (3.7)$$

The GRM Equation is subjected to two boundary conditions when solving chromatographic problems. The first boundary condition states that transport to the inlet occurs only through convection, while transport from the inlet
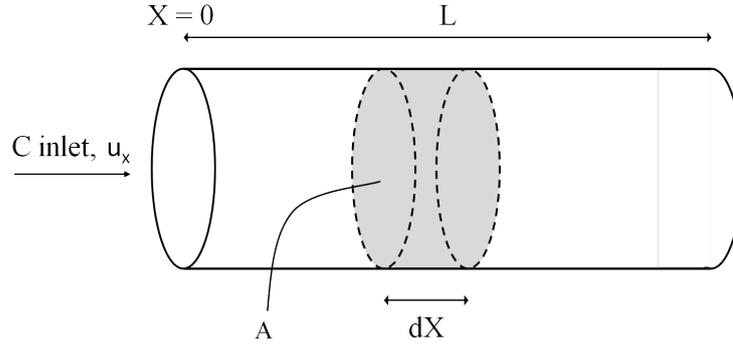
Figure 3.1: A thin slice of the column, over which the mass balance is formulated

occurs through convection and dispersion. This is presented as a mass balance over the volumeless inlet in Eq. 3.8. Accumulation does not occur in this surface.

$$u_0 A \varepsilon_c c_{inlet} = u_0 A \varepsilon_c c - D_{A,x} \varepsilon_c A \frac{\partial C}{\partial x} \quad \text{at } x = 0 \tag{3.8}$$

Equation 3.8 can be rearranged to give the common Robin condition that describes the column inlet.

$$\frac{\partial C}{\partial x} = \frac{u_0}{D_{A,x}}(c - c_{inlet}) \quad \text{at } x = 0 \tag{3.9}$$

The second boundary condition is over the column outlet interface, at x=L. Both convective and dispersive transports are taken into consideration at the outlet, whereas only convective transport is considered as leaving the outlet. The concentration is assumed to be the same on both sides of the interface and the following mass balance can be obtained:

$$u_0 A \varepsilon_c c_{inlet} - D_{A,x} \varepsilon_c A \frac{\partial C}{\partial x} = u_0 A \varepsilon_c c \quad \text{at } x = L \tag{3.10}$$

which can be rearranged into 3.11, a Neumann condition at the outlet of the column.

$$\frac{\partial C}{\partial x} = 0 \quad \text{at } x = L \tag{3.11}$$

3.2   The particle

The resistance to mass transfer from the surface of the particles to sites of adsorption is described by D_e, the effective diffusion coefficient (m^2/s). Transport within particles can be modeled using a mass balance over a thin radial element of the particle. The particle is assumed to be a sphere of radius R (m) and r is a variable shell radius $(0 < r \leq R)$. The thickness of the radial element is δr (see fig. 3.2). The mass balance is written as:

$$IN = OUT + ACCUMULATION + ADSORPTION \tag{3.12}$$

For simplification, the particle porosity, ϵ_p and the diffusivity are assumed to be independent of the position in the particle. The various terms in Equation 3.12 are:

$$ACC = 4\pi r^2 \varepsilon_p \cdot \Delta r \cdot \frac{\partial C_p}{\partial t} \tag{3.13}$$

$$(IN - OUT)_{Diff} = \left(-D_e \varepsilon_p 4\pi r^2 \frac{\partial C_p}{\partial r}\right)_r - \left(-D_e \varepsilon_p 4\pi r^2 \frac{\partial C_p}{\partial r}\right)_{r+\Delta r} \tag{3.14}$$

$$ADSORPTION = (1 - \varepsilon_p)4\pi r^2 \Delta r \frac{\partial q}{\partial t} \tag{3.15}$$

C_p is the concentration in the pore liquid (mol/m^3) and $\frac{\partial q}{\partial t}$ is the adsorption rate $(mol/m^3_{solid}s)$. Putting together Equations: 3.12-3.15 gives the following expression:

$$\left(-D_e \varepsilon_p 4\pi r^2 \frac{\partial C_p}{\partial r}\right)_r - \left(-D_e \varepsilon_p 4\pi r^2 \frac{\partial C_p}{\partial r}\right)_{r+\Delta r} -$$
$$(1 - \varepsilon_p)4\pi r^2 \Delta r \frac{\partial q}{\partial t} = 4\pi r^2 \varepsilon_p \cdot \Delta r \cdot \frac{\partial C_p}{\partial t}$$

Division by $4\pi r^2 \varepsilon_p \Delta r$ and letting $\Delta r \to 0$ gives Equation 3.16 which describes the mass transport within the porous sorbent particles.
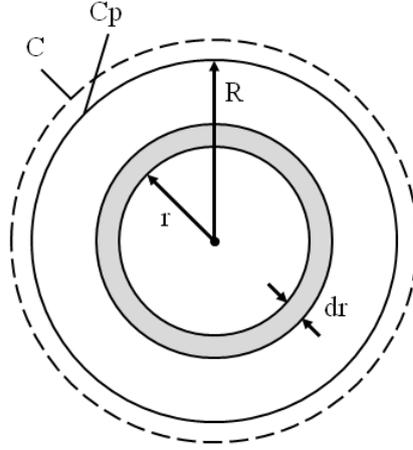
Figure 3.2: Shell balance of a thin slice of a sorbent particle

$$\frac{\partial C_p}{\partial t} = D_e \left(\frac{\partial^2 C_p}{\partial r} + \frac{2}{r} \frac{\partial C_p}{\partial r} \right) + \frac{1 - \varepsilon_p}{\varepsilon_p} \frac{\partial q_i}{\partial t} \tag{3.16}$$

This particle model has two boundary conditions. In the first boundary condition, the transport of a component between the particle surface and its surrounding is assumed to take place in a thin film surrounding the particle. Transport from the bulk phase to the particle is then described by 3.17

$$4\pi R^2 \varepsilon_p \cdot k_c(c - c_{p,R}) \ \text{ at } r = R \tag{3.17}$$

Transport between the surface of the particle and the interior of the particle is a diffusive process. The diffusive flux from the surface to the interior is described by 3.18

$$D_e \varepsilon_p 4\pi R^2 \frac{\partial C_p}{\partial r} \ \text{ at } r = R \tag{3.18}$$

Since there is neither production nor accumulation on the surface, the mass balance of the surface is:

$$4\pi R^2 \cdot k_c(c - c_{p,R}) = D_e \varepsilon_p 4\pi R^2 \frac{\partial C_p}{\partial r} \ \text{ at } r = R \tag{3.19}$$

Equation 3.19 is equivalent to a Robin condition and is commonly written

$$\frac{\partial C_p}{\partial r} = \frac{k_c}{D_e}(c - c_{p,R}) \ \text{ at } r = R \tag{3.20}$$

At the particle centre there is no net flux, thus; the concentration gradient equals zero, i.e. a Neumann condition.

$$\frac{\partial C_p}{\partial r} = 0 \ \text{ at } r = 0 \tag{3.21}$$

3.3   Summary of the mathematical model

Equations describing the transport of a component in a fixed bed flow and the relevant boundary conditions are summarized below. The equations listed describe the effects of axial dispersion, $D_{A,x}$, film mass transfer resistance, k_C, effective particle diffusion, D_e, and a non-linear adsorption rate equation model. Equation 3.22 describes the bulk liquid phase in the column with boundary conditions according to 3.23 at the inlet and outlet, respectively.

$$\frac{\partial C}{\partial t} = -u_0\frac{\partial C}{\partial x} + D_{A,x}\frac{\partial^2 C}{\partial x} - \frac{1-\varepsilon_c}{\varepsilon_c}\frac{6}{d_p}k_c\left(C - C_s\right) \tag{3.22}$$

$$\frac{\partial C}{\partial x} = \begin{cases} \frac{\nu}{D_e}(c - c_{in}) & \text{at x} = 0 \\ 0 & \text{at x} = \text{L} \end{cases} \tag{3.23}$$

Equation 3.24 describes the fluid-phase concentration in the particles with the boundary condition according to 3.25 at the particle surface and particle centre, respectively.

$$\frac{\partial C_p}{\partial t} = D_e\left(\frac{\partial^2 C_p}{\partial r} + \frac{2}{r}\frac{\partial C_p}{\partial r}\right) + \frac{1-\varepsilon_p}{\varepsilon_p}\frac{\partial q_i}{\partial t}\cdot H_i \tag{3.24}$$

$$\frac{\partial C_p}{\partial r} = \begin{cases} \frac{k_c}{D_e}(c - c_p) & \text{at r} = \text{R} \\ 0 & \text{at r} = 0 \end{cases} \tag{3.25}$$

The form of Equation 3.24 assumes that the adsorbed species are located in the solid phase. In Equation 3.24 the parameter H_i has been added to describe the adsorption effect by adjusting the concentration of organic solvent in the mobile phase.

3.4 Numerical

The General Rate Model (GRM), Equations 3.22-3.25, consisting of a set of partial differential equations (PDEs) were solved numerically using the method of lines. The PDEs were discretized to generate a set of Ordinary Differential Equations (ODEs). The set of ODEs was solved using the predefined function ODE15s in Matlab, an implicit, multistep NDF method (Shampine and Reichelt [26]). A fourth-order central finite difference scheme was used for solving both the axial and the particle domains.

Grid independence of the model was tested with simulations of the full model with the particle radius discretized in 15, 25 and 40 equally spaced volumes. 25 points of discretization were chosen as sufficient in the later simulations, as a tradeoff between precision and computational time. The axial domain was discretized into 200 equally spaced volumes for the same reason as the particle radius.

4

Experimental techniques

4.1 Paper I – Separation of wood constituents

In Paper 1, a simple method for fractionating lignin, hemicelluloses and LCCs from hot-water-extracted Norway spruce was tested. The idea was to separate the constituents according to hydrophobicity, i.e. the relative amount of aromatic groups.

Sawdust of Norwegian Spruce wood was extracted batch wise in autoclaves. The procedure was adapted according to Song et al. [27] to dissolve material with a preference for the low molecular region; 1-10 kDa.

A cross-flow filtration pilot plant was used for the fractionation of the hot-water extract. The system was operated batch wise and circulated the suspension across the filter several times. The main advantage of using cross-flow filtration instead of dead-end filtration is that no filter cake is formed. The two membrane filters used were designed with cut offs at 1 and 5 kDa, respectively.

The preparative sorption setup consisted of a glass container containing the suspension, connected via plastic tubing to a high performance liquid chromatography (HPLC) pump. The pump, in turn, was connected via a stainless steel capillary to the column, packed with hydrophobic resin. The outlet of the column was connected to a glass container to collect the permeate or eluate. The processes of filtration and sorption are illustrated in Figure 4.1. Two different resins were used; a polymeric resin, Amberlite XAD-16, with a styrene
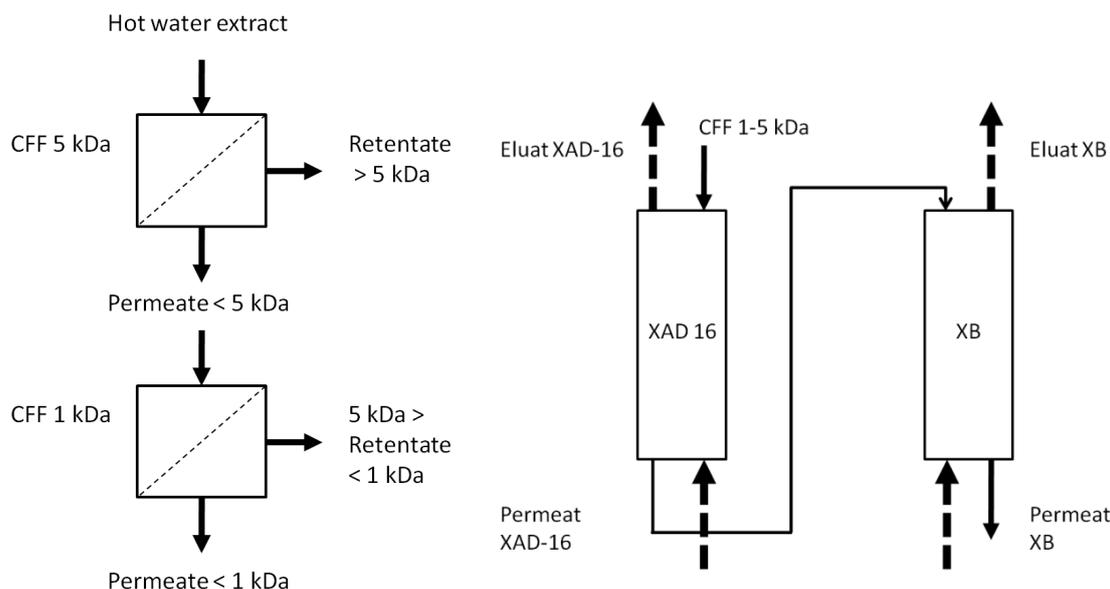
Figure 4.1: Experimental setup

divinylbenzene structure, was packed in a 7.8×300 mm steel column. The second column was an analytical chromatography column; XBridge Phenyl 5 μm (4.6×250 mm). The columns were used in the order depicted in Figure 4.1. The loading and elution steps were performed with low flow rates to ensure that the fluid had time to penetrate the voids in the particles. In the washing sequences, however, the flow rate was increased to the maximum capacity of the pump. The sorptive procedure was executed in a batch-wise sequence to assure that the capacity of the column was not exceeded. The sequence was: Load - Wash - Elution - Wash.

To characterize the fractions, Klason lignin and sugar content were determined according to the TAPPI test method (1987) T222 OM-83, slightly modified to autoclave at elevated temperature and pressure. For a more comprehensive description of the analytical procedure, see Wigell et al. [28]. The acid-soluble lignin was quantified using spectrophotometry. The molecular weight distribution of the fractions was determined with size exclusion chromatography in a phosphate buffer. Enzymatic hydrolysis of LCCs was carried out with the enzyme NS-51023, Novozymes. The activity of the enzyme had previously been tested according to the method described in Lawoko et al. [29], resulting in verified high hydrolysis on glucomannan and no activity on either lignin,

pectin, CMC, or xylan (Y. Wang, pers. comm.).

A more detailed description of the equipment and material can be found in
Paper I.

4.2   Paper II - Mathematical modeling and parameter estimation

Experimental setup

All breakthrough and pulse injection experiments were performed in a high
performance liquid chromatography (HPLC) setup. For detection; a dual wave-
length UV detector and an evaporative light scattering detector (ELSD) were
used.

Model compounds and solvents

The model system in this work was meant to resemble the separated species
in Paper I to as great an extent as possible. To be able to distinguish the
effect of various parameters, the model compounds must be in pure fractions.
Obtaining hemicelluloses with a monodispersed degree of polymerization (DP)
and carrying an exact number of aromatic side groups is difficult, especially
if a higher DP is desired. In order to overcome this obstacle, the effect of
DP on the retention mechanism was neglected, and instead, focus was on the
aromatic/hydrophobic character of the model compounds.

Salicin is a flavanoid and was chosen as model compound due to its similar-
ities to LCCs: a sugar monomer with an aromatic side group. Veratryl alcohol
(3,4-Dimethoxybenzyl alcohol) was used as a model compound for lignin in this
study. Veratryl alcohol is soluble in water and methanol and is more strongly
hydrophobic in character than salicin. The chemical structures of these model
compounds are illustrated in Figure 4.2.

Blue dextran (Mw 2.000 kDa) is a very large, inert polymer that was used
when determining bed porosity and axial dispersion since it cannot penetrate
the pores of the particles.

In Westerberg et al. [30] acetonitrile was found to be the favorable organic
solvent, while the model compounds used in this work displayed higher solu-

bility in methanol. Therefore, throughout the work, methanol was used as the organic modifier instead of acetonitril.
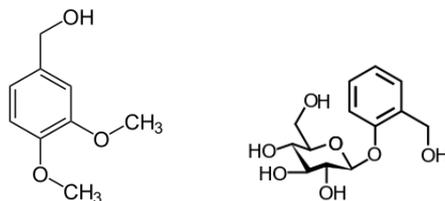
Figure 4.2: Left: veratryl alcohol, right: salicin

Resins and columns

The advantage of using large particle sorbents is the reduction in pressure drop, which allows for a higher production rate in preparative separation. Two batches of granular silica, one with and one without phenyl ligands, were used in this work. The particle size distribution was measured using laser diffraction, and the result is presented in Figure 4.3.

Two porosities were estimated in this work; bed porosity, ε_c, and particle porositiy, ε_p. Bed porosity is defined as the void space of the packed column, excluding the void inside the particles. This porosity was estimated by generating breakthrough curves of Blue Dextran, 2MDa, which is too large to penetrate the pores of the particles. The breakthrough curves were generated at several flow rates and an average porosity was estimated from these volumes.

Particle porosity refers to the porous void volume inside the particles and
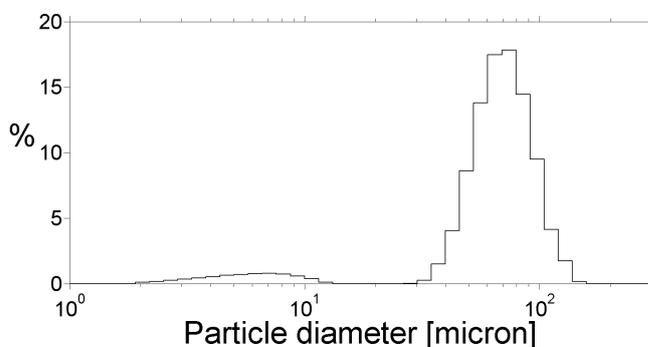
Figure 4.3: Particle diameter distribution

was estimated using the same procedure as above, except using smaller, inert molecules that penetrate and diffuse through the particles.

In addition to these experiments, the solid density of the untreated silica and the phenylic silica was determined using pycnometer measurements. With the solid density the total porosity, ε_{tot} can be determined.

Phenylic silica was loaded in a 4.6×250 mm and a 4.6×75 mm column. The untreated silica was loaded in a 4.6×250 mm column. A vibratory device was used to assist the formation of the bed.

Estimation of parameters

The axial dispersion parameter was estimated by parameter fitting Equation 3.22, without the third term on the right-hand side, to experimental data of pulse injections of Blue Dextran. Pulse injection chromatograms were generated with and without the silica column connected to the system. The pulse injection generated without column connected to the system was used as input in the simulation. The dispersion parameter in Equation 3.22 was fitted to the generated dispersed pulse. Only the top 80 % of the peaks were used in the fitting, since a tailing effect was observed, which was interpreted as meaning that the tracer interacted with the sorbent particles.

The diffusivity of the species was estimated using the correlation developed by Wilke and Chang [21], Equation 2.21. For comparison, the diffusivity was also estimated using the Stokes-Einstein equation, Equations 2.19 - 2.20. According to the work of Wilke and Chang [21], as pertains to the solvents used and the molecular weight of the species, the Wilke-Chang equation was expected to be more accurate than the Stokes-Einstein equation.

The film mass transfer resistance was estimated using the well known Wilson-Geankoplis correlation (Wilson and Geankoplis [19]), Equation 2.18. The polydispersed particle size distribution makes the use of such a correlation uncertain. The impact of a faulty k_c value was tested with the full model in the verification trials.

A parameter H_i was introduced in Equation 3.24, to account for the effect on
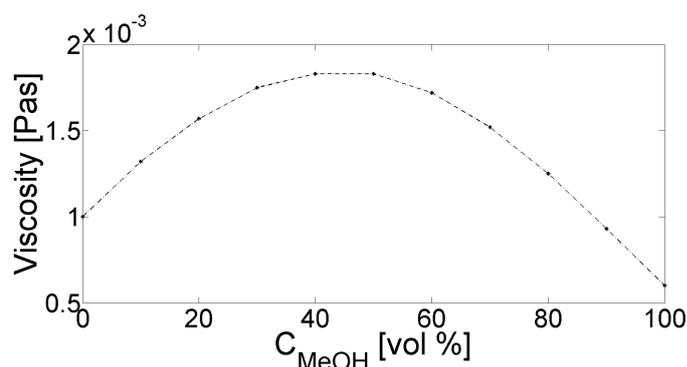
Figure 4.4: Solvent viscosity, effect of MPM-concentration.

the adsorptivity of solutes to changes in the concentration of organic modifier in the mobile phase. The effect of organic solvent concentration on the hydrophobic affinity of the analytes was examined using isocratic retention time measurements of pulse injections, with varying concentrations of methanol. The full model (Equations 3.22 - 3.25), including H_i, was fitted to match the retention time of the highest peak. The H_i values were then plotted against methanol concentration and a curve was fitted to that slope.

In addition to affecting the affinity of the solute for the liquid phase, the mixture of methanol-water has a different viscosity than the pure solvents. The true viscosity of the solvent was estimated by interpolating the data presented in Snyder et al. [31], neglecting the pressure effect on viscosity. The effect of pressure on liquid-state viscosity in methanol-water mixtures has been examined by Kubota and Tsuda [32] who found this effect to be of minor importance. The values of viscosity were taken at $20\,^{\circ}$C. The viscosity effect of the solvent mixture is illustrated in Figure 4.4.

The equilibrium concentration of the solutes in adsorbed state was measured using breakthrough experiments. The area above the generated breakthrough curve was integrated and a breakthrough volume was calculated by subtracting the column void and the integrated breakthrough curve generated with no column connected to the system. The total mass adsorbed was calculated with the known liquid phase concentration. The curve of q_i moles adsorbed to c_i moles/L bulk was then fitted to a number of known adsorption isotherms. After fitting the parameters of the isotherms, the isotherm showing the least residual

to the experimental values was used in the model.

4.2.1   Numerical

The parameter estimation was based on the MatLab function lsqnonlin, a non-linear least-squares method, which minimizes the residual between the experimental breakthrough curve and the simulated by adjusting the parameters to be estimated in small steps and moving towards the steepest gradient. The inlet to the column in the simulation was the experimental values from injections performed with no column connected to the system.

5

Results and discussion

5.1 Paper I

The objective of the investigation was to test the potential and limitations in a simple laboratory setup to separate hot-water-extracted wood constituents into fractions of hemicelluloses, lignin and lignin-carbohydrate complexes. The main results are presented in Table 5.1.

The complete separation procedure produced three fractions; a retentate on the XAD-16 sorbent, a retentate on the phenylic XB sorbent, and the material that was able to permeate both sorbents without being retained. Throughout the result section these three fractions will be called HWE-XAD, HWE-XB, and HWE-GGM. Hot-water extract, filtered at 1-5 kDa, and the permeate of the XAD sorbent are included in the analysis as points of reference, and are referred to as HWE-CFF and HWE-XAD-P.

Fraction	Aromatics [wt%]	Yield [mg/g dry wood]
HWE-CFF	5.5	49
HWE-XAD	55.7	1.8
HWE-XB	10.2	1.4
HWE-GGM	1.5	23.7 *

Table 5.1: Summary of main results. * *Estimated from TDS measurements.*

Fraction	Ara	Gal	Glu	Xyl	Man	Klason	ASL
HWE-CFF	3.01	10.42	15.01	11.74	59.82	4.17	1.42
HWE-XAD	1.04	7.32	16.31	2.41	72.92	52.78	2.94
HWE-XAD-P	3.17	10.86	14.72	12.66	58.59	1.02	0.88
HWE-XB	0.20	4.55	18.46	0.55	76.24	8.48	1.71
HWE-GGM	3.42	11.61	14.30	13.99	56.68	0.85	0.69

Table 5.2: Sugar composition in % of total sugars. Klason lignin and acid soluble lignin in wt-% of TDS.

The hot water extraction yielded 144 mg total dry solids (TDS) per gram dry wood (OD) after high mesh filtration. After cross-flow filtration the remaining TDS amounted to 49 mg g^{-1} where the dead volume of the equipment accounted for a loss of 7.5 mg g^{-1}. The final yield on extract was thus 34 % which confirms that the HWE conditions chosen could dissolve material in this region, as suggested by Song et al. [27]. About 44 % of the TDS was lost in the 1 kDa permeate in cross-flow filtration.

The composition of sugars, Klason lignin and acid soluble lignin in each fraction are presented in Table 5.2.

The proportion of Man/Glc remained constant at about 4 in all fractions, Table 5.2, which is in agreement with the Norway spruce glucomannan findings of Willfor et al. [33]. Both galactose and arabinose were strongly reduced in content in the retained fractions. About 12 % of the original sugars were xylans. Very small amounts of the xylans were, however, found in the retentates, which led us to believe that the extracted xylan and arabinogalactan were not bound to lignin. However, previous analyses of lignin carbohydrate complexes in spruce have shown that lignin is bound to both xylan and glucomannan (Lawoko [34]. Thus, it is our belief that a major part of the xylan-lignin complex in spruce wood cannot be extracted with hot water at the conditions applied in this work. This is not strange, as the impediment to the quantitative extraction of hemicelluloses with hot water has partly been attributed to part of them being covalently bonded to a macromolecular hydrophobic lignin in wood (Tunc et al. [35]; Chen et al. [36]).

The sugar composition remained fairly constant in a comparison of the permeates through adsorptive separation; HWE-CFF to HWE-DAX-P, and HWE-GGM. Data consistently showed that the sugars enriched in the retained

fractions were reduced in the permeate fraction and vice versa. In both re-
tentates, mannose and glucose were enriched, whereas arabinose, xylose and
galactose were enriched in the permeates. Following the assumption of Willfor
et al. [37] that all mannose was present in galactoglucomannan with a ratio of
mannose:glucose:galactose of 4:1:0.5, the sugar part of the HWE-GGM fraction
consisted of about 79 % GGM, and the remainder was xylan and arabinogalac-
tan in the ratio of 2:1.

75.5 % of the Klason lignin and 38 % of the ASL entering the first sorbent
were retained in the HWE-XAD fraction. The XB sorbent reduced the Klason
lignin content by 16.6 % and the remainder of the ASL by 21.6 %. The total
reduction of Klason lignin was 79.6 % , and the total reduction of ASL was
51.4 %.

The calculated degree of detection, i.e. detectable sugars and lignin, was 80
to 85 % in all fractions. The low degree of detection is likely due to a combina-
tion of various measurement errors, mostly attributed to undetected inorganic
material in the samples.

Characterization

The HWE-XAD fraction contained mainly lignin, but also a significant amount
of sugars. It is our belief that the fraction consisted of a mix of lignin con-
stituents, LCCs with a high degree of aromatic side groups, and possibly also
hemicelluloses that have been sterically retained in the porous particles and
eluted with the adsorbed constituents.

The HWE-GGM fraction was shown to consist of mainly sugars. The small
amounts of lignin material found in this fraction could be LCCs with a very
low degree of aromatic side groups, thus with high aqueous solubilty, and not
retained on a hydrophobic resin.

To confirm the existence of covalent bonds between lignin and carbohydrates
in the HWE-XB fraction, the method of Lawoko et al. [29] was employed. Size-
Exclusion Chromatography (SEC) was used to estimate the molecular weight
(M_W) of the polymers in the HWE-XB fraction before and after enzymatic
hydrolysis. The enzyme used is specific in cleaving the mannose-mannose bonds
that make up the polymeric backbone of glucomannanas. The elution time of
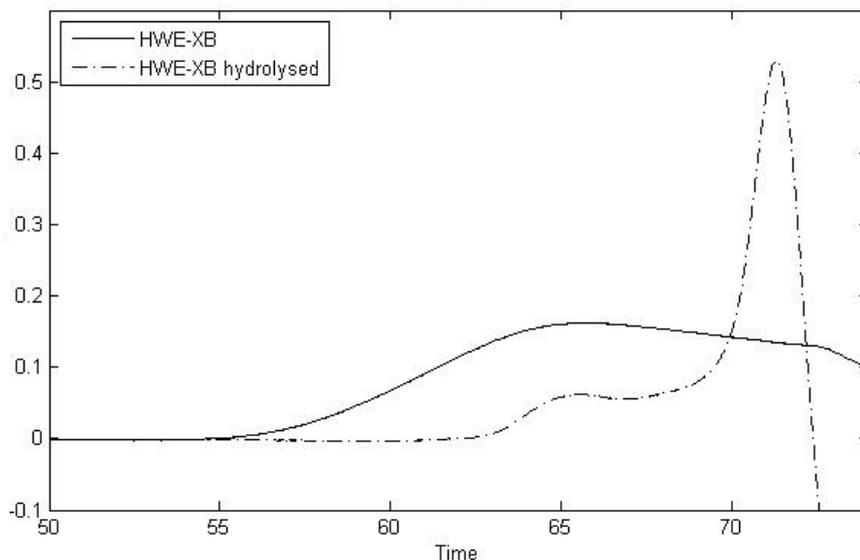
Figure 5.1: HP-SEC curve of HWE-XB fraction. UV detector signal at 280 nm

the UV_{280} absorbing species was monitored and a shift towards a lower M_W of these species was observed after enzymatic hydrolysis, Figure 5.1. Since the enzyme had reduced the molecular weight of the molecules, without any ligninase activity, this means that the UV_{280} absorbing species must have been bound to the carbohydrates that were degraded.

5.1.1   Discussion

The simple method of fractionating wood constituents using filtration and sorption tested in this work proved successful. Three fractions were obtained and characterized according to the fraction´s main constituent as either lignin, hemicellulose or LCC. However, the study also pointed out the limitations of the method. The sorptive sequence of load-wash-elution-wash was very time consuming in order to maintain the purity of the fractions. In relation to this, the pressure drop over the columns increased significantly during prolonged use. Upon dismantling the columns the inlet and outlet frits were noticed to have been severely fouled. Cleansing the frits in heated 0.5 M alkali for 30 minutes removed all visible fouling, and the pressure drop was restored to its original level. A proper sequence in preparative separation should thus also include a cleansing stage. In order to reduce the cycle time, it seems necessary

to include an intermediate separation stage prior to the sorptive sequence to remove large lignin structures and inorganic matter, which are suspected of being the fouling species.

Moreover, further insight into the sorption behaviour of the species and the transport mechanisms that take place in the column is needed for design and operation purposes.

5.2   Paper II

The objective of the investigation was to develop a mathematical model for chromatographic separation of wood constituents and to estimate the values of transport and adsorption parameters for two model compounds. The resulting parameter values are presented in the text, which is followed by a discussion of the results.

The silica-based sorbents are manufactured as granular particles, which is a rather crude product - unsuitable for analytical chromatography. The reduced specificity of the sorbent is, however, made up for by a strongly reduced manufacturing cost, which could become a significant cost factor in large-scale applications. Another significant aspect is that a larger particle diameter is necessary in large-scale applications to reduce the pressure drop over the column. In this aspect there is a tradeoff between flow rate/production rate and the dispersion mechanisms that reduces separation efficiency.

The values of porosities and particle diameter that was used in the model are summarized in Table 5.3.

The values presented in table 5.3 are the ones used in modeling. However; salicin exhibited less than expected retention in the phenylic columns. Comparing the Stoke´s radius to the mean pore diameter of the sorbent particles

Sorbent	Column	ε_C	ε_p	$d_p[\mu m]$
Phenyl	4.6×250	0.35	0.39	68
Phenyl	4.6×75	0.35	0.39	68
Silica	4.6×250	0.35	0.59	68

Table 5.3: Final particle and column parameters used in model

reveals that the particle penetration must be hindered, especially in the case of the slightly larger molecule salicin. To account for the restricted particle penetration of salicin an efficiency factor is introduced: $\alpha_{Sal} = 0.83$. This value is obtained by assuming that adsorption/desorption is rapid in comparison to mass transfer, thus neglecting adsorption kinetics totally and fitting the particle porosity to the retention time of a low concentration injection of salicin in pure methanol.

The results from estimation of axial dispersion are summarized in Figure 5.2, where Equation 5.1 is plotted with the experimental values. Parameter fitting of pulse injection curves resulted in a linear curve for the narrow Re interval investigated. The curve was in the same range as predicted by Chung and Wen [18], Equation 2.11, but increased more rapidly with increasing Reynolds number.

$$D_{A,x} = 2.97 \cdot 10^{-6} \cdot Re + 0.127 \cdot 10^{-6} \qquad m^2/s \qquad (5.1)$$
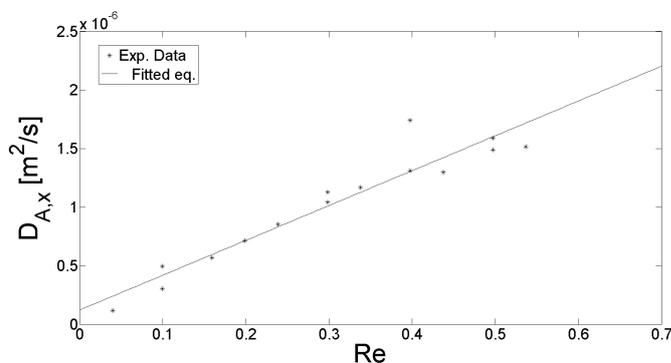
Figure 5.2: Axial dispersion as a function of Reynolds number

The results from calculating the diffusivities from the method of Wilke and Chang [21] are presented in Table 5.4. According to Wilke and Chang [21], as pertains to solvent and solute properties, the Stokes-Einstein correlation underestimates diffusivity, resulting in values about one order of magnitude lower.

The H_i values fitted to retention time measurements are plotted in Figure 5.3 along with the fitted Equation 5.2. Equation 5.2 was adapted from Melander et al. [38]. It is an Equation that includes both hydrophobic and electrostatic

Solvent	Veratryl	Salicin
Water	7.5	6.1
Methanol	8.5	7.0

Table 5.4: Diffusivities in $\times 10^{-10}\ m^2/s$
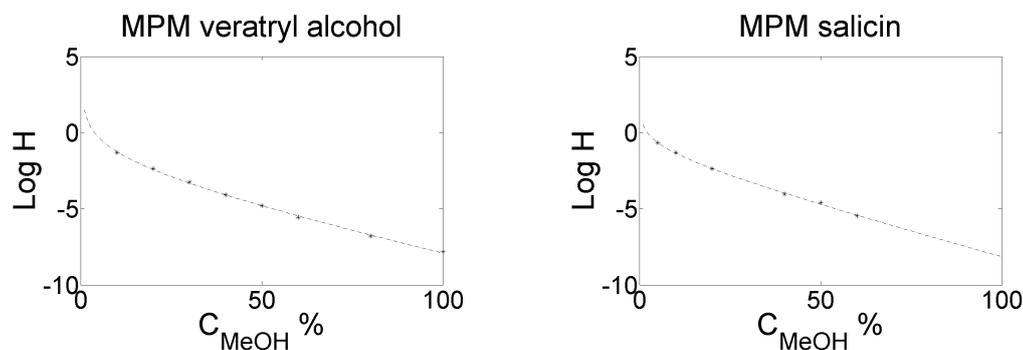
Figure 5.3: Effect of mobile phase modifier. Left: veratryl alcohol, right: salicin

interaction. While this physical interpretation might be somewhat inaccurate for this system, the expression fits the experimental values well.

$$log(H_i) = \alpha_1 + \alpha_2 log(C_{MeOH}) + \alpha_3 C_{MeOH} \tag{5.2}$$

The adsorption equilibrium data was fitted to several known isotherms. A 3-parameter isotherm proved necessary to fit the data, and the Tóth isotherm showed the best fit, Equation 2.8. The fitted isotherms of the species are plotted with the experimental data in Figure 5.4. The Tóth isotherm reduced to the Henry type Equation at low concentrations, which was used in simulations to avoid numerical difficulties.

Verification of the model

The verification of the model developed was done experimentally on the 75×4.6 mm phenylic silica column. The experimental pulse injections were compared to the corresponding curve simulated with the model. The model was verified by estimating the error in the predicted elution volume. Furthermore, the shapes of the injection pulse and the corresponding simulated curve were compared and the possible sources of inconsistency were listed.
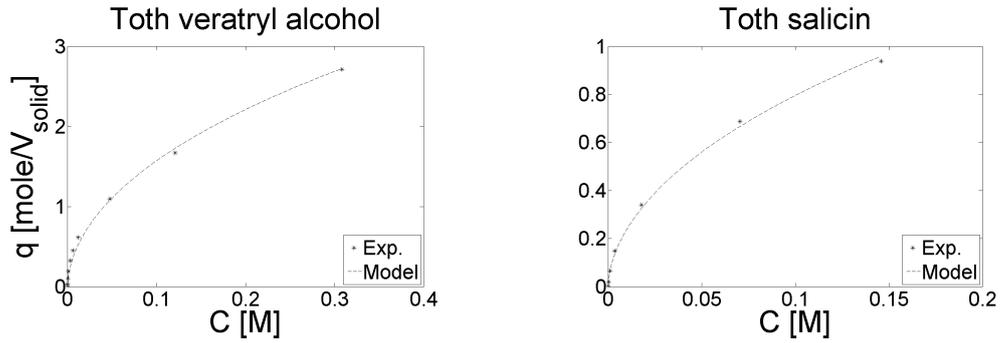
Figure 5.4: Tóth isotherms of veratryl alcohol and salicin

The elution volume error average was calculated with Equation 5.3.

$$\overline{R} = \frac{\sum |1 - t_{r,sim}/t_{r,exp}|}{n} \qquad (5.3)$$

where t_r is the retention time of the highest peak for the simulated and experimental pulse, respectively, and n is the number of experiments. The model was found to be accurate to within 95 %, in regard to the elution volume.

With the parameters estimated individually, the simulated peak shape was close to perfectly Gaussian. The experimentally generated peaks, however, exhibited a *fronting* behaviour, where a part of the peak eluted at a lower volume than the calculated. This observed phenomena was interpreted as *channeling*. An alternative explanation is that some of the particle pores had been plugged, or *fouled*, which would have a similar effect on the peak shape.
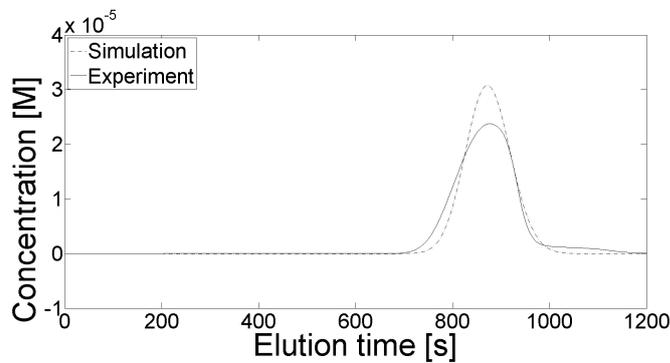
Figure 5.5: Example of simulation versus experimental elution

5.2.1   Discussion

The objective of this work was to create a mathematical model of chromato-graphic separation of wood constituents for a simplified model system. The purpose of the model is to evaluate how various parameters influence this sepa-ration and, with this knowledge, to find the optimal operational conditions for preparative separation.

The Biot number was used to compare external with internal mass transfer resistance (Equation 2.14. k_c varied with the flow rate, while the particle diam-eter was fixed in the investigation and D_e varied only slightly with the solvent. The Biot number was in the range of 10-20 in this work, which means that the internal mass transfer resistance was dominant.

The kinetics of adsorption/desorption has been neglected in this work. This simplification was suggested by Ruthven [16] who argues that the physical adsorption-/desorption rates are much faster than internal and external mass transfer rates. The hydrophobic affinity to the stationary phase was stronger for veratryl alcohol than for salicin, as predicted by Westerberg et al. [30] and Takahashi et al. [39]. The solubility in mixtures of water and methanol is well described by the mobile phase modifier parameter; H_i. The estimated adsorption isotherms match the experimental values well, and the column- and particle porosities, ε_c and ε_p, were determined using two methods. The weakest part of the model seems to be the mechanical dispersion effect. The verification tests showed that the elution curves were fronting. A comparison of the elu-tion volume to the column volume confirmed that this was not a kinetic effect. The effect is called "*channeling*", but whether the origin of this is in the bed structure or in the particle pores is unclear.

The system of chromatographic separation of wood constituents was, in this work, largely simplified in order to be able to evaluate the individual parameters of separation. Only one type of sorbent material, one kind of organic solvent, and only two model compounds were selected to resemble the constituents of wood. The largest deviation of the model from a real case separation procedure

lies in the chemical structure of the constituents. The lignin-carbohydrate bonding scheme is not well understood, and the structure of the water soluble lignin fragments, produced when dissolving wood, are complex and diverse. The number of aromatic side groups of the LCCs controls the adsorption on a hydrophobic resin, as shown by Takahashi et al. [39] and Westerberg et al. [30], while the molecular weight of the molecules has a major influence on which sorbent geometry to use and then, especially, the diffusivity of the species. The value of the biopolymers increases by molecular weight (M_w) and purity (monodisperse aromaticity), which makes high demands on processing costs. The model created in this work is intended to be used to find the optimal tradeoff between processing cost and purity and the limitations of the process.

6

Conclusions and Outlook

6.1 Conclusions

This study has shown that it is possible to separate hemicelluloses, lignin and LCCs by means of hydrophobic sorption. An experimental study applied cross-flow filtration followed by two sequential stages of hydrophobic sorption on a water suspension of wood polymers. This process separated the species according to their respective hydrophobicity. The species were characterized and quantified using sugar analysis, Klason analysis, acid soluble lignin measurements and by using size exclusion chromatography (SEC) combined with enzymatic hydrolysis. The SEC method was employed to confirm the existence of covalent linkages between aromatic and carbohydrate constituents. The hot-water-extraction procedure extracted wood polymers with a preference for the desired degree of polymerisation, and additional purification with cross-flow filtration removed both particulate matter and low molecular weight material. The affinity of the solutes for the stationary phase was regulated by using two different sorbents. The low hydrophobicity of the LCCs and the very low hydrophobicity of hemicelluloses allowed these polymers to pass through the first column, while the lignin molecules were adsorbed. The second column had stronger hydrophobicity and was therefore able to adsorb most of the LCC polymers. The resulting hemicellulose fraction contained about 1 % aromatics, the LCC fraction contained about 10 % aromatics and the lignin fraction contained about 56 % aromatics.

The separation method presented here is a simple and non-destructive method for separating wood constituents in rather crude fractions.

To be able to resolve the parameters that influence the separation, a simplified model system was constructed. Model compounds were used to resemble lignin and LCC. The parameters that describe chromatographic separation were determined by combining experiments with parameter fitting. In addition, the equilibrium concentration of the model compounds in a phenylic silica sorbent in relation to their concentration in pure water was measured and fitted to the Tóth isotherm. The solubility effect of the organic solvent concentration in the mobile phase was determined and a parameter describing the effect was derived. The internal mass transfer resistance was found to dominate the total mass transfer resistance in the region of experiments. The mathematical model developed was proven to be accurate to 95 %. Furthermore, calculations of the Stokes radius of the model compounds revealed the particle pore radius to be a limiting factor, especially considering that wood polymers are much larger than the model compounds used in this work.

An example of how the model can be used is illustrated in Figure 6.1. A specific *case* of preparative chromatographic separation was simulated. Veratryl alcohol and salicin were injected at a low concentration onto a 4.6 mm diameter column. The flow rate was fixed at 0.2 ml/min and the mobile phase consisted of 50/50 v/v % MeOH/water. The separation requirement was set to 95 % purity of salicin, which was eluted first. Figure 6.1 shows the elution curves of the two solutes, and the volume to be collected is highlighted by dotted lines.

The simulated separation procedure produced salicin of 95 % purity and a yield of 94.3 %. Furthermore, the column length required for this specific case was calculated to be 25.5 mm and the estimated pressure drop over this column was 1.45 bar. This is the optimal bed geometry for the given operating conditions.
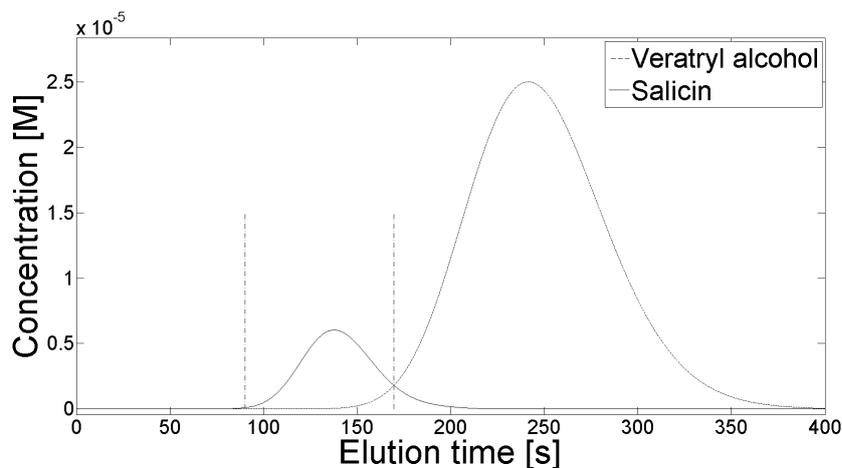
Figure 6.1: Example of optimisation of preparative chromatography

6.2   Future work

Future work will focus on additional simulations to establish the limiting parameters of chromatographic separation. One priority will be the development of an optimization method, pertaining to purity and yield. Other aspects will be included in a later stage, including parameters such as solvent requirements and the pressure drop over the packed bed.

It would be of great interest to measure the parameters presented in Westerberg and Rasmuson [40] using compounds of greater resemblance to native wood constituents. Of particular interest is the effect of a higher degree of polymerisation and of various extents of aromatic side groups. The suspension used in Westerberg et al. [30] is too dispersed in these aspects to distinguish individual parameters, while the model compounds in Westerberg and Rasmuson [40] are probably too simplified representations of the actual wood polymers of interest.

Bibliography

[1] ASPO, www.aspousa.org, 2012.

[2] WWSC, www.wwsc.se, 2010.

[3] M. S. Lindblad, E. Ranucci, A. C. Albertsson, Macromolecular Rapid Communications 22 (2001) 962–967.

[4] M. Grondahl, L. Eriksson, P. Gatenholm, Biomacromolecules 5 (2004) 1528–1535.

[5] J. Hartman, A. C. Albertsson, J. Sjoberg, Biomacromolecules 7 (2006) 1983–1989.

[6] A. Bjorkman, Nature 174 (1954) 1057–1058.

[7] T. Koshijima, T. Watanabe, Association between lignin and carbohydrates in wood and other plant tissues, Springer Velag, Berlin, Heidelberg, New York,, 2003.

[8] J. Azuma, N. Takahashi, T. Koshijima, Carbohydrate Research 93 (1981) 91–104.

[9] M. Lawoko, G. Henriksson, G. Gellerstedt, Holzforschung 60 (2006) 156–161.

[10] Y. Uraki, Y. Usukura, T. Kishimoto, M. Ubukata, Holzforschung 60 (2006) 659–664.

[11] P. Oinonen, in: Proceedings of the 16th ISWFPC, Tianjin.

[12] T. Persson, H. Krawczyk, A. K. Nordin, A. S. Jönsson, Bioresource Technology 101 (2010) 3884–3892.

[13] A. Andersson, T. Persson, G. Zacchi, H. Stalbrand, A. S. Jonsson, Applied Biochemistry and Biotechnology 137 (2007) 971–983.

[14] S. H. Lin, R. S. Juang, Journal of Environmental Management 90 (2009) 1336–1349.

[15] M. Ek, Ljungberg textbook. Pulp and paper chemistry and technology. Book 2, Pulping chemistry and technology, Fiber and Polymer Technology, KTH, Stockholm, 2007.

[16] D. Ruthven, Principles of Adsorption and Adsorption Processes, Wiley, New York, 1984.

[17] G. Guiochon, A. Felinger, D. Shirazi, A. Katti, Fundamentals of Preparative and Nonlinear Chromatography, Elsevier, San Diego, CA, 2006.

[18] S. F. Chung, C. Y. Wen, AIChE Journal 14 (1968) 857–866.

[19] E. J. Wilson, C. J. Geankoplis, Industrial & Engineering Chemistry Fundamentals 5 (1966) 9–14.

[20] A. Fick, Annalen der Physik und Chemie 170 (1855) 59–86.

[21] C. Wilke, P. I. N. Chang, A.I.Ch.E. Journal (1955) 264–270.

[22] M. Suzuki, Adsorption Engineering, Elsevier, Amsterdam, 25 vol edition, 1990.

[23] H. Darcy, Les Fontaines Publiques de la Ville de Dijon, Victor Dalamont, Paris, 1856.

[24] T. H. Chilton, A. P. Colburn, Trans. Am. Inst. Chem. Eng. 26 (1931).

[25] S. Ergun, Chemical engineering progress 48 (1952).

[26] L. F. Shampine, M. W. Reichelt, SIAM J. SCI. COMPUT. 18 (1997) 1–22.

[27] T. Song, A. Pranovich, I. Sumerskiy, B. Holmbom, Holzforschung 62 (2008) 659–666.

[28] A. Wigell, H. Brelid, H. Thellander, Nordic Pulp & Paper Research Journal 22 (2007) 495–499.

[29] M. Lawoko, A. Nutt, H. Henriksson, G. Gellerstedt, G. Henriksson, Holz-forschung 54 (2000) 497–500.

[30] N. Westerberg, H. Sunner, M. Helander, M. Lawoko, G. Henriksson, A. Rasmuson, BioResources 7 (2012) 4501–4516.

[31] L. R. Snyder, J. J. Kirkland, J. W. Dolan, Introduction to Modern Liquid Chromatography, Oxford: Wiley-Blackwell, 3 edition, 2010.

[32] B. Y. H. Kubota, S. Tsuda, THE REVIEW OF PHYSICAL CHEMISTRY OF JAPAN 49 (1979).

[33] S. Willfor, R. Sjoholm, C. Laine, M. Roslund, J. Hemming, B. Holmbom, Carbohydrate Polymers 52 (2003) 175–187.

[34] M. Lawoko (2005).

[35] M. S. Tunc, M. Lawoko, A. van Heiningen, Bioresources 5 (2010) 356–371.

[36] X. W. Chen, M. Lawoko, A. van Heiningen, Bioresource Technology 101 (2010) 7812–7819.

[37] S. Willfor, P. Rehn, A. Sundberg, K. Sundberg, B. Holmbom, Tappi Journal 2 (2003) 27–32.

[38] W. R. Melander, Z. E. Rassi, C. Horváth, Journal of Chromatography A 469 (1989) 3–27.

[39] N. Takahashi, J. I. Azuma, T. Koshijima, Carbohydrate Research 107 (1982) 161–168.

[40] N. Westerberg, A. Rasmuson, Chromatographic separation of wood model constituents - Mathematical modeling and parameter estimation, 2013.